Journal of Nuclear Medicine, published on July 31, 2020 as doi:10.2967/jnumed.120.246785

Preclinical Development of ^{18}F-OF-NB1 for Imaging GluN2B-Containing N-Methyl-D-Aspartate Receptors and its Utility as a Biomarker for Amyotrophic Lateral Sclerosis

*Hazem Ahmed[1], Rahel Wallimann[1], Ahmed Haider[1], Vahid Hosseini[2], Stefan Gruber[1], Marvin Robledo[1], Thi A. N. Nguyen[1], Adrienne Müller Herde[1], Irina Iten[1], Claudia Keller[1], Viola Vogel[2], Roger Schibli[1,3], Bernhard Wünsch[4], Linjing Mu[1,3], Simon M. Ametamey[1]**

[1]Institute of Pharmaceutical Sciences, ETH Zurich, Vladimir-Prelog-Weg 4, CH-8093 Zurich, Switzerland

[2]Laboratory of Applied Mechanobiology, Institute of Translational Medicine, Department of Health Sciences and Technology, ETH Zürich, Vladimir-Prelog-Weg 4, CH-8093 Zurich, Switzerland

[3]Department of Nuclear Medicine, University Hospital Zurich, CH-8091 Zurich, Switzerland

[4]Institute of Pharmaceutical and Medicinal Chemistry, University of Münster, D-48149 Münster, Germany

Corresponding author:
Prof. Dr. Simon M. Ametamey
Radiopharmaceutical Sciences
Institute of Pharmaceutical Sciences
ETH Zurich
Vladimir-Prelog-Weg 4
CH-8093 Zurich
Phone: +41 44 6337463
Fax: +41 44 6331367
simon.ametamey@pharma.ethz.ch

First author:
Mr. Hazem Ahmed
PhD student
Radiopharmaceutical Sciences
Institute of Pharmaceutical Sciences
ETH Zurich
Vladimir-Prelog-Weg 4
CH-8093 Zurich
Phone: + 41 44 6333962
hazem.ahmed@pharma.ethz.ch

Word count: 4978

Short running title: Noninvasive PET imaging of GluN2B subunits

This project was supported by the Swiss National Science Foundation Grant Nr. 310030E_160403/1 and 310030E_182872/1.

ABSTRACT

As part of our continuous efforts to develop a suitable fluorine-18 labeled positron emission tomography (PET) radioligand with improved imaging characteristics for imaging the GluN2B-bearing *N*-Methyl-D-aspartate receptors (NMDARs), we investigated in the current work *ortho*- and *meta*-fluorinated analogues of ^{18}F-PF-NB1, a 3-benzazepine-based radiofluorinated probe. **Methods**: OF-NB1 and MF-NB1 were prepared using a multi-step synthesis and their binding affinities towards GluN2B subunits and selectivity over sigma-1 receptors (σ1Rs) were determined via competitive binding assays. ^{18}F-OF-NB1 was synthesized via copper-mediated radiofluorination, and was evaluated in Wistar rats by *in vitro* autoradiography, PET imaging, *ex vivo* biodistribution, metabolite experiments and receptor occupancy studies using CP-101,606, an established GluN2B antagonist. To determine *in vivo* selectivity, ^{18}F-OF-NB1 was validated in wild-type and σ1R knock-out mice. Translational relevance was assessed in autoradiographic studies using postmortem human brain tissues from healthy individuals and ALS patients, the results of which were corroborated by immunohistochemistry. **Results**: The binding affinity values for OF-NB1 and MF-NB1 towards the GluN2B subunits were 10.4±4.7 nM and 590±36 nM, respectively. For σ1R binding, OF-NB1 and MF-NB1 exhibited K_i values of 410 nM and 2700 nM, respectively. OF-NB1, which outperformed MF-NB1, was radiolabeled with ^{18}F to afford ^{18}F-OF-NB1 in > 95% radiochemical purity and molar activities of 192±33 GBq/μmol. In autoradiography experiments, ^{18}F-OF-NB1 displayed a heterogeneous and specific binding in GluN2B subunit-rich brain regions such as the cortex, striatum, hypothalamus and hippocampus. PET imaging studies in Wistar rats showed a similar heterogeneous uptake, and no brain radiometabolites were detected. A dose-dependent blocking effect was observed with CP-101,606 (0.5-15 mg/kg) and resulted in a D_{50} of 8.1 μmol/kg. Postmortem autoradiography results revealed a lower expression level of the GluN2B subunits in ALS brain tissue sections compared to healthy controls, in line with immunohistochemistry results. **Conclusion**: ^{18}F-OF-NB1 is a highly promising PET imaging probe for imaging the GluN2B subunits of the NMDAR. It possesses utility for receptor occupancy studies and has potential for PET imaging studies in ALS patients and possibly other brain disorders.

Keywords: NMDA, GluN2B-subunit, positron emission tomography (PET), receptor occupancy, amyotrophic lateral sclerosis (ALS)

INTRODUCTION

N-Methyl-D-aspartate receptors (NMDARs) are one of three glutamate ion channel types prevalent in the central nervous system and are key players in synaptic transmission, plasticity and higher cognitive functions (*1*). Once NMDARs, particularly extrasynaptic ones, are over-activated due to uncontrolled glutamatergic stimulation, an apoptotic cascade is triggered rendering L-glutamate a neurotoxin in a pathological process known as excitotoxicity (*2*). This deleterious event was found to be involved in several neurodegenerative and psychiatric diseases such as Alzheimer's disease, vascular dementia, Parkinson's disease, depression, stroke and schizophrenia (*3*). The discovery of GluN2B subunit-containing NDMARs as major contributors to glutamate-mediated excitotoxicity and the allosteric ifenprodil-binding pocket situated at the interface of GluN1 and GluN2B channeled drug development strategies towards subunit-selective antagonists (*4*). These emerging drugs possess similar activity of non-selective NMDARs antagonists but exhibit a favorable safety profile relative to their non-selective predecessors (*5*). Nonetheless, a number of promising GluN2B-subunit antagonists such as CERC-301 (MK-0657) were assessed in clinical trials showing no-to-modest benefit-risk ratio (*6*). As such, pivotal tools for the efficient evaluation of drug-target engagement and occupancy are of highest priority (*7*). Non-invasive positron emission tomography (PET) imaging modality is such a tool that can be used in preclinical and clinical settings to assess drug-target engagement, receptor occupancy (RO) and therapy monitoring.

Despite more than two decades of research efforts, no suitable clinical GluN2B-subunit PET imaging agent currently exists due to one or more major shortcomings such as brain radiometabolites, considerable off-target binding especially to sigma-1 receptors (σ1Rs), low brain uptake and brain uptake inconsistent with known GluN2B expression profile (*8-11*). Recently, our group successfully developed (*R*)-^{11}C-Me-NB1, a 3-benzazepin-1-ol derived GluN2B-subunit PET radiotracer lacking the aforementioned limitations (*12*) and is currently being assessed in a first-in-human clinical trial. The major inherent limitation of this tracer is the short physical half-life of carbon-11 (physical half-life = 20.3 min), which impedes its usage in imaging centers without an on-site cyclotron. The development of a fluorine-18 (physical half-life = 109.8 min) radiolabeled GluN2B-subunit PET tracer would offer satellite distribution and higher image resolution (*13*). Our initial endeavors yielded (*R*)-^{18}F-OF-Me-NB1, a fluorine-18 analogue of Me-NB1 (*14*) which despite the encouraging preclinical results, displayed a relatively fast brain washout. Nevertheless, two characteristics were explicated from this published study; *ortho*-fluorination on the phenyl ring critically impacted the affinity of the tracer towards GluN2B subunits whilst *para*-fluorination led to a loss of affinity. The second evident

characteristic was that the (*R*)- enantiomer of ^{18}F-OF-Me-NB1 was superior to the (*S*)- enantiomer as shown by its specific and selective behavior towards GluN2B subunit-containing NMDARs. At the time, it was also reported that 3-(4-phenylbutyl)-2,3,4,5-tetrahydro-1*H*-benzazepine-1,7-diol exhibits 18-fold higher GluN2B subunit affinity when compared to its methoxy analogue (*15*). Remarkably, we showed in our previous study that the loss of high binding affinity and selectivity of the *para*-fluorinated 3-benzazepin-1-ol (PF-Me-NB1) could be restored upon cleavage of the methyl ether group (*16*). More importantly, we found that the (*S*)- and (*R*)-enantiomers of PF-NB1 did not differ in their *in vitro* properties with regard to their binding affinity and selectivity towards GluN2B subunits.

As part of our continuous efforts to develop a suitable fluorine-18 labeled PET radioligand for imaging the GluN2B subunits of the NMDAR, we investigated in the current work *ortho*- and *meta*-fluorinated analogues of PF-NB1 (Figure 1) in an effort develop an imaging agent with improved imaging characteristics. Following the synthesis and the *in vitro* validation of both compounds, OF-NB1 was selected for subsequent radiofluorination, and further *in vitro* and *in vivo* evaluation. To showcase the utility of this novel tracer, RO studies were performed in rats applying CP-101,606, a GluN2B antagonist. Furthermore, we evaluated in a pilot study a possible *in vivo* interaction or off-target binding of ^{18}F-OF-NB1 to σ1Rs using the σ1 ligand, fluspidine, and σ1R knock-out (σ1-KO) mice. Finally, for the purpose of clinical translation, we assessed the binding properties of ^{18}F-OF-NB1 on postmortem human brain tissues obtained from amyotrophic lateral sclerosis (ALS) patients using *in vitro* autoradiography, the results of which were exemplary confirmed by immunohistochemistry (IHC) and analyzed by confocal microscopy.

MATERIALS AND METHODS

The organic syntheses of the reference compounds and precursors were performed in analogy to our previously published protocols with minor modifications for the precursor synthesis (Supplemental Figures 1 and 2) (*14*). Animal experiments were accomplished in accordance with the Swiss Animal Protection Law and the Animal Research: Reporting of In Vivo Experiments (ARRIVE) guidelines after authorization from the local veterinary office of the Canton Zurich in Switzerland. The preparation of glass slides for autoradiography and confocal microscopy was performed at the Institute of Veterinary Pathology, University of Zurich. Wistar rats were acquired from Charles River, while CD1 and σ1R-KO mice were acquired from Envigo (Barcelona, Spain) and all were retained under standard conditions as previously reported (*17*). Human ALS and non-ALS brain tissue was obtained from the National Institute of Health (NIH) NeuroBioBank and Harvard Brain Tissue Resource Center. The need for informed consent for brain tissues was waived under local and national law given that the tissue samples were anonymized. Metabolite and biodistribution studies were conducted as previously described (*14*). Log$D_{7.4}$ of ^{18}F-OF-NB1 was determined using the shake-flask method in n-octanol/phosphate-buffered saline at pH 7.4.

Chemistry and Binding Affinity Determination

Chemicals and materials were purchased from ABCR, Amatek Scientific, Armar, Merk, Sigma Aldrich, Acros Organics and Perkin Elmer and were used directly without any further purification. Detection, characterization and binding affinity experiments were performed in accordance with previously published procedures (*16*).

Radiochemistry

The radiosynthesis of ^{18}F-OF-NB1 was performed using boronic ester 6 in analogy to a previously published procedure by our group (Supplemental Figure 3) (*16,18*). The radiosynthesis of ^{18}F-fluspidine was performed as previously reported (*19*).

In vitro Autoradiography

In vitro autoradiography was carried out as previously described by our group (*14,16*). For blocking experiments, 1 μM of GluN2B ligands of either CERC-301 or EVT-101 were used. For off-target binding, 1 μM of σ1R ligands, SA4503 and fluspidine were employed.

Metabolite Study

Wistar rats were injected intravenously with 249-599 MBq (2.74-4.70 nmol/kg) of ^{18}F-OF-NB1. Brain extracts at 15, 30, and 60 min, and blood samples at 5, 15, 30, 45, and 60 min post-injection were acquired, processed and analyzed by radio-UPLC as previously described by our group (*14,16*).

Ex vivo Biodistribution

Eight male Wistar rats (4 baseline and 4 blockade animals) were administered via tail-vein injection of ^{18}F-OF-NB1 (16-22 MBq, 0.31-0.42 nmol/kg), either alone or shortly after the injection of 2 mg/kg of eliprodil, and the rats were sacrificed by decapitation under isoflurane anesthesia at 45 min post-injection and processed as previously described by our group (*14,16*).

In vivo PET and Dose Response Studies

CD1 and σ1R-KO mice as well as Wistar rats were anesthetized with isoflurane and were imaged with a PET/CT scanner (Super Argus; Sedecal) upon tail-vein injection of ^{18}F-OF-NB1 or ^{18}F-fluspidine. Either 28-45 MBq (0.42-8.10 nmol/kg) of the radiotracers were injected into rats or 15-17 MBq (2.54-18.51 nmol/kg) into mice with a scan time of 90 min. Dose–response and RO studies were accomplished in Wistar rats by tail-vein injection of different doses (0.5, 3.0, 10 and 15 mg/kg) of CP101,606. For the cross-talk studies in mice, the GluN2B blocker (*R*)-Me-NB1 (2 mg/kg), σ1 receptor blockers fluspidine (1 mg/kg) and SA4503 (2.5 mg/kg) were employed. All blockers were administered 1 min prior to radiotracer injection. The acquired data was reconstructed as previously reported (*17*). Time–activity curves (TACs) were produced by PMOD (version 3.9; PMOD Technologies) with predefined volumes of interest using an MRI T2 template.

Fluorescence Immunostaining, Confocal Microscopy and Image Analysis

For fluorescence staining, 10 μm thick ALS and non-ALS frozen brain tissue sections were washed with phosphate-buffered saline (PBS) and then fixed in 4% paraformaldehyde in PBS for 30 min. Non-specific adsorption of antibody was prevented by adding bovine serum albumin (2% w/v, 30 min). After washing the samples for 3x with PBS, tissues were incubated with primary antibody anti-NMDAR2B (1/100) for 1 h at room temperature (Abcam, [N59/36] (ab93610)). Samples were then washed 3x with PBS and treated with a secondary antibody (Goat anti-Mouse Alexa-Fluor 633 from Invitrogen, USA) with a dilution of 1:500 in PBS for 1 h at rt. Cell nuclei were stained by DAPI (2μg/ml, 10 min). Samples were finally washed 3x with PBS, mounted in mounting media and imaged using a confocal microscope (Olympus FV1000, Japan).

Pixel by pixel signal intensity images analysis was performed while maintaining the imaging conditions identical for samples to be compared. This analysis was performed to compare intra- (in different regions of the tissue) and inter- (between different samples) expression of GluN2B. The mean intensities from selected parts of an image were measured using ImageJ and the average intensity of images was plotted for each condition.

Statistical Analysis

An independent two-tailed Student's test of the dataset was employed to calculate statistical probability values, assuming normal distribution.

RESULTS

Chemistry and Binding Affinity

Modifications introduced for the synthesis of boronic ester precursor 6 resulted in an overall yield of 11%, a seven-fold increase compared to the original route. MF-NB1 on the other hand, was obtained in 14%. Inhibition constants (K_i) for OF-NB1 and MF-NB1 towards the GluN2B subunits and σ1Rs were determined using competitive binding assays with ^{3}H-ifenprodil and (+)-^{3}H-pentazocine, respectively, and are summarized in **Table 1**.

Radiolabeling

The radiosynthesis of ^{18}F-OF-NB1 was accomplished using aryl boronic ester precursor 6 in an average total synthesis time of 140 min from end of bombardment (Figure 2). The isolated radiochemical yield of ^{18}F-OF-NB1 was 5.5±0.1% (*n*=6) with radiochemical purity >95%. Molar activity amounted to 192±33 GBq/μmol (*n*=6). Log$D_{7.4}$ was found to be 2.18±0.06 (*n*=5), which is an optimal value for passive brain entry (*20*). The radiochemical yield obtained for ^{18}F-fluspidine was similar to reported values and was formulated in saline as previously described (*19*).

In vitro Autoradiography

A representative autoradiogram obtained with ^{18}F-OF-NB1 is depicted in Figure 3. ^{18}F-OF-NB1 showed a heterogeneous binding with high accumulation in brain areas such as cortex, striatum, thalamus and hippocampus, brain regions known to have high densities of the GluN2B subunits (*5*). The cerebellum, a region with low GluN2B-subunit expression, exhibited negligible radioactivity accumulation. GluN2B antagonists blocked the accumulation of ^{18}F-OF-NB1 while σ1R blockers, on the other hand, did not compete with ^{18}F-OF-NB1.

Dose-dependency and Receptor Occupancy Studies in Wistar Rats

^{18}F-OF-NB1 exhibited excellent blood-brain barrier penetration in line with the measured Log$D_{7.4}$ value of 2.18. Under baseline conditions, a heterogeneous accumulation in the rat brain, consistent with GluN2B-subunit expression pattern was observed (Supplemental Figure 4). In Figure 4 are shown coronal, sagittal and axial averaged images of the rat brain under baseline and blockade conditions. Radioactivity uptake was reduced in a dose-dependent

manner using the GluN2B subunit antagonist CP-101,606 as reflected by the respective TACs in Figure 5A. The standard uptake values (SUVs) from the blocking studies were employed to calculate *in vivo* RO of CP-101,606 (Figure 5B). A dose of 8.1 μmol/kg was required to achieve 50% RO.

Ex vivo Metabolite Study

The metabolite analysis revealed only intact parent radiotracer in the brain 60 min post-injection as shown in Supplemental Figure 5.

Ex vivo Biodistribution Studies

GluN2B subunit-rich brain regions such as cortex, striatum, thalamus and hippocampus exhibited high accumulation of radioactivity compared to regions with poor expression of the GluN2B-subunits, i.e. cerebellum. Values for the normalization of GluN2B-rich regions to cerebellum were as follows: cortex/cerebellum (1.39±0.03), striatum/cerebellum (1.25±0.03), thalamus/cerebellum (1.22±0.06), and hippocampus/cerebellum (1.03±0.02). In the periphery, specific accumulation was highest in the adrenal gland, to which previous reports repudiated the presence of GluN2B subunits in the adrenal gland (*21*). On the other hand, other regions such as the brain stem and midbrain showed high and specific accumulation. Biodistribution results are summarized in Supplemental Tables 1 and 2.

PET Imaging in CD1 and σ1-KO Mice

Injection of 1 mg/kg fluspidine caused a reduction of radioactivity uptake of ^{18}F-OF-NB1 (Figure 6A) in both CD1 and σ1R-KO mice. Uptake of ^{18}F-fluspidine, on the other hand in both CD1 and σ1R-KO mice, was substantially different (Figure 6B); a rapid washout in the σ1R-KO mouse was observed, whereas a slow washout and persistently high TACs were observed in the CD1 mice. Specificity of binding was confirmed by using another σ1R ligand, SA4503 (2.5 mg/kg), as a blocker. Furthermore, when 2 mg/kg of (*R*)-Me-NB1 was used as a blocker in CD1 mice, a blocking effect was observed.

Autoradiography and Confocal Microscopy using Postmortem Human Brain Tissue

In postmortem human brain tissue samples of ALS patients, we found a lower accumulation of ^{18}F-OF-NB1 compared to non-ALS brain tissues in the cortical brain regions, BA4 and BA6, in autoradiographic experiments (Figure 7A). To confirm that this is not confounded by neuronal loss, we further performed fluorescence

immunostaining and confocal imaging of the postmortem human brain cryosections. For the confocal microscopy, semi-quantitative signal intensity analysis of the images was performed and the level of GluN2B subunit expression was normalized to cell nuclei count. Overall, the results of the analysis of the immunostained images (n=10) showed a significantly lower expression of GluN2B and no neuronal loss in brain tissues of ALS patients compared to non-ALS subjects ($P<0.01$, Figure 7B). Furthermore, we also found that in areas with higher cell nuclei density (> 150 cells/10^6 μm^2) which are most likely cortical regions of the brain, the expression of GluN2B was relatively homogenous in non-ALS brain sections and significantly higher ($P<0.0001$) compared to ALS patient brain sections.

DISCUSSION

^{18}F-PF-NB1, a 3-benzazepine-1,7-diol derivative published recently by our group, is by far the best performing radiofluorinated tracer in view of its favorable *in vivo* profile in rodents (*16*). In the current work, we investigated whether shifting the fluorine atom from the *para*-position in PF-NB1 to the *ortho*-and *meta*-positions in the phenyl ring, termed OF-NB1 and MF-NB1 respectively, would have any major impact on the *in vitro* and *in vivo* binding properties. While MF-NB1 showed low affinity and selectivity towards GluN2B subunits, OF-NB1 displayed superior *in vitro* binding properties, and was therefore selected for radiofluorination. PET imaging findings of ^{18}F-OF-NB1 in rats corroborated the *in vitro* autoradiography results whereby a heterogeneous and high radioactivity uptake was observed in GluN2B-rich regions. The D_{50} value obtained from the CP-101,606 RO studies was similar to the values observed in previous studies. The TACs were also similar to those of ^{18}F-PF-NB1 (*12,16*). ^{18}F-OF-NB1 established its superiority over ^{18}F-PF-NB1 in *ex vivo* biodistribution studies, in which case higher target-to-cerebellum accumulation ratios were achieved. However, ^{18}F-OF-NB1 showed specific binding in low GluN2B-expression regions such as midbrain, brain stem and cerebellum in line with previous reports (*12,14,16,17*). Whether this is a GluN2B-related specific binding or an off-target binding remains to be investigated. The administration of CP101,606 caused an initial surge in the brain uptake of ^{18}F-OF-NB1, which may be explained by the increased availability of unbound tracer arising from blockade of peripheral GluN2B-bearing NMDA receptors.

Using GluN2B KO mice is an elegant method to investigate the potential *in vivo* interaction or off-target binding of ^{18}F-OF-NB1 towards σ1Rs, however, homozygous GluN2B KO are not viable (*22*). Alternatively, σ1R-KO mice, which survive for a relatively long period of time can be employed. Based on our previously reported cross-talk experiments, we hypothesized that the administration of a σ1R ligand would alter the binding of ^{18}F-OF-NB1 in wild-type mice, but not in σ1R-KO mice given the absence of σ1R modulation (*17*). To modulate σ1Rs, we selected fluspidine since the fluorine-18 labeled version is an established PET radioligand for imaging σ1Rs (*19*). As anticipated, injection of 1 mg/kg fluspidine in CD1 mice caused a reduction of radioactivity accumulation of ^{18}F-OF-NB1. Surprisingly, a similar blocking effect was observed in the σ1R-KO mice, which cannot be attributed to σ1R modulation (Figure 6A). Possible explanations could be off-target binding of fluspidine to GluN2B subunits, or that σ1R-KO mice are not entirely devoid of σ1Rs. For the purpose of validating the σ1R-KO mice, we administered ^{18}F-fluspidine into wild-type CD1 and σ1R-KO mice. A fast washout of ^{18}F-fluspidine was observed in the brain of σ1R-

KO mice, indicating the absence of σ1Rs and off-target binding of ^{18}F-fluspidine (Figure 6B). In order to probe the off-target potential of the 3-benzazepine series, we applied (*R*)-Me-NB1, a selective GluN2B subunit ligand (*12*). Unexpectedly, a dose of 2 mg/kg of (*R*)-Me-NB1 showed a substantial blocking effect comparable to 2.5 mg/kg of SA4503, a σ1R ligand. From these studies, we concluded that fluspidine in concentrations of 1 mg/kg might exhibit off-target binding toward GluN2B subunit-containing NMDARs, and that the observed effects are not necessarily an exclusive consequence of cross-talk between σ1R and GluN2B-containing NMDARs. Similar blocking effects with SA4503 were observed in a recent publication with another GluN2B radioligand, ^{11}C-(*S*)-NR2B-Me (*23*). This is also valid for some GluN2B ligands such as (*R*)-Me-NB1 where off-target binding toward σ1Rs becomes more prominent at high concentrations. For future cross-talk imaging experiments with different σ1R agonists, one should consider the use of wild-type CD1/σ1R-KO mice pair, as done in this study, in order to exclude the direct effect of the σ1R agonists on GluN2B-containing NMDARs. Additionally, we suggest that future σ1R *in vitro* binding experiments should not solely focus on σ1/σ2R selectivity, but should also take into account the off-target binding affinity to GluN2B subunits.

Given our ultimate goal of clinical translation, we explored the expression level of GluN2B subunits in postmortem human brain cortex tissues of ALS patients and healthy controls using *in vitro* autoradiography. Glutamatergic excitotoxicity is described as one of the contributing factors to the susceptibility of the motor neurons to neurodegeneration in ALS (*24*). Supporting evidence suggested changes in the expression of GluN2B subunit-containing NMDARs in mouse and rat models of ALS (*25,26*) and therefore, for our investigations, we selected ALS as a disease model for neurodegeneration. In particular, two sub-cortical regions (motor and frontal, BA4 and BA6 areas) were selected for this experiment. We found a decreased accumulation of the tracer in tissues from ALS patients compared to healthy volunteers. This decreased accumulation was further corroborated with IHC as shown by confocal microscopy, suggesting that GluN2B subunit levels can be measured in ALS patients undergoing GluN2B-related treatments.

CONCLUSION

^{18}F-OF-NB1 has been developed as a front-runner of our first generation radiofluorinated ligand, (*R*)-^{18}F-OF-Me-NB1. It showed favorable *in vitro* and *in vivo* attributes in terms of GluN2B subunits specificity, selectivity over σ1Rs, metabolism and kinetics. Its utility for drug development was demonstrated in a RO study with CP-101,606, wherein a dose dependency of radioligand uptake was observed. Off-target binding of GluN2B ligands to σ1Rs and vice versa is a potential confounder when developing drugs targeting these receptors or studying the featured *in vivo* cross-talk between both receptors. Finally, *in vitro* autoradiography using ALS and healthy postmortem human brain tissues revealed a decreased accumulation of ^{18}F-OF-NB1 in GluN2B-rich regions in ALS patients when compared to healthy controls. This finding indicates possibly a substantial GluN2B subunit downregulation, which was confirmed by IHC. Overall, the results suggest that ^{18}F-OF-NB1 is a promising GluN2B radioligand with utility for RO studies and PET imaging studies in patients with ALS, and potentially also for other neurodegenerative diseases not investigated in this study.

.

DISCLOSURE

The authors declare no conflict of interest.

ACKNOWLEDGMENTS

We would like to thank NIH NeuroBioBank and Harvard Brain Tissue Resource Center for supplying ALS and healthy postmortem human brain tissue. This project was supported by the Swiss National Science Foundation Grant Nr. 310030E-160403/1 and 310030E_182872/1 to Prof. S. M. Ametamey. Dr. Jose Miguel Vela is acknowledged for providing our group with the σ1R-KO mice.

Key Points

QUESTION: Can we selectively image GluN2B subunit-containing NMDARs with ^{18}F-OF-NB1 *in vitro*/*in vivo*, and can GluN2B-targeted imaging serve as a diagnostic marker for ALS?

PERTINENT FINDINGS: PET imaging in Wistar rats using ^{18}F-OF-NB1 showed a heterogeneous uptake in GluN2B-rich brain regions that could be blocked in a dose-dependent manner by the GluN2B antagonist, CP-101,606, and autoradiography experiments using postmortem cortical brain tissue revealed lower GluN2B subunits in ALS patients compared to healthy controls, which was in line with immunohistochemistry results.

IMPLICATIONS FOR PATIENT CARE: ^{18}F-OF-NB1 has the potential to detect GluN2B subunits in patients with neurodegenerative diseases, especially in ALS patients and also has utility for RO studies in humans.

REFERENCES

1. Dingledine R, Borges K, Bowie D, Traynelis SF. The glutamate receptor ion channels. *Pharmacol Rev.* 1999;51:7-61.

2. Sattler R, Tymianski M. Molecular mechanisms of calcium-dependent excitotoxicity. *J Mol Med (Berl).* 2000;78:3-13.

3. Hardingham GE, Bading H. Synaptic versus extrasynaptic NMDA receptor signalling: implications for neurodegenerative disorders. *Nat Rev Neurosci.* 2010;11:682-696.

4. Perin-Dureau F, Rachline J, Neyton J, Paoletti P. Mapping the binding site of the neuroprotectant ifenprodil on NMDA receptors. *J Neurosci.* 2002;22:5955-5965.

5. Mony L, Kew JN, Gunthorpe MJ, Paoletti P. Allosteric modulators of NR2B-containing NMDA receptors: molecular mechanisms and therapeutic potential. *Br J Pharmacol.* 2009;157:1301-1317.

6. Addy C, Assaid C, Hreniuk D, et al. Single-dose administration of MK-0657, an NR2B-selective NMDA antagonist, does not result in clinically meaningful improvement in motor function in patients with moderate Parkinson's disease. *J Clin Pharmacol.* 2009;49:856-864.

7. Kemp JA, McKernan RM. NMDA receptor pathways as drug targets. *Nat Neurosci.* 2002;5 Suppl:1039-1042.

8. Fuchigami T, Nakayama M, Yoshida S. Development of PET and SPECT probes for glutamate receptors. *ScientificWorldJournal.* 2015;2015:716514.

9. Gruber S, Ametamey SM. Imaging the glutamate receptor subtypes—Much achieved, and still much to do. *Drug Discov Today Technol.* 2017;25:27-36.

10. Fu H, Tang W, Chen Z, et al. Synthesis and preliminary evaluations of a triazole-cored antagonist as a PET imaging probe ([18F]N2B-0518) for GluN2B Subunit in the Brain. *ACS Chem Neurosci.* 2019;10:2263-2275.

11. van der Aart J, Yaqub M, Kooijman EJM, et al. Evaluation of the novel PET tracer [11C]HACH242 for imaging the GluN2B NMDA receptor in non-human primates. *Mol Imaging Biol.* 2019;21:676-685.

12. Haider A, Herde AM, Krämer SD, et al. Preclinical evaluation of benzazepine-based PET radioligands (R)- and (S)-11C-Me-NB1 reveals distinct enantiomeric binding patterns and a tightrope walk between GluN2B- and σ1-receptor–targeted PET imaging. *J Nucl Med.* 2019;60:1167-1173.

13. Ametamey SM, Honer M, Schubiger PA. Molecular imaging with PET. *Chem Rev.* 2008;108:1501-1516.

14. Haider A, Iten I, Ahmed H, et al. Identification and preclinical evaluation of a radiofluorinated benzazepine derivative for imaging the GluN2B subunit of the ionotropic NMDA receptor. *J Nucl Med*. 2019;60:259-266.

15. Börgel F, Szermerski M, Schreiber JA, et al. Synthesis and pharmacological evaluation of enantiomerically pure GluN2B selective NMDA receptor antagonists. *ChemMedChem.* 2018;13:1580-1587.

16. Ahmed H, Haider A, Varisco J, et al. Structure–affinity relationships of 2,3,4,5-tetrahydro-1H-3-benzazepine and 6,7,8,9-tetrahydro-5H-benzo[7]annulen-7-amine analogues and the discovery of a radiofluorinated 2,3,4,5-tetrahydro-1H-3-benzazepine congener for imaging GluN2B subunit-containing N-Methyl-d-aspartate receptors. *J Med Chem.* 2019;62:9450-9470.

17. Kramer SD, Betzel T, Mu L, et al. Evaluation of (11)C-Me-NB1 as a potential PET radioligand for measuring GluN2B-containing NMDA receptors, drug occupancy, and receptor cross talk. *J Nucl Med.* 2018;59:698-703.

18. Preshlock S, Calderwood S, Verhoog S, et al. Enhanced copper-mediated 18F-fluorination of aryl boronic esters provides eight radiotracers for PET applications. *Chem Commun (Camb).* 2016;52:8361-8364.

19. Fischer S, Wiese C, Maestrup EG, et al. Molecular imaging of sigma receptors: synthesis and evaluation of the potent sigma1 selective radioligand [18F]fluspidine. *Eur J Nucl Med Mol Imaging.* 2011;38:540-551.

20. Pike VW. PET radiotracers: crossing the blood-brain barrier and surviving metabolism. *Trends Pharmacol Sci.* 2009;30:431-440.

21. Schwendt M, Jezova D. Gene expression of NMDA receptor subunits in rat adrenals under basal and stress conditions. *J Physiol Pharmacol.* 2001;52:719-727.

22. Kutsuwada T, Sakimura K, Manabe T, et al. Impairment of suckling response, trigeminal neuronal pattern formation, and hippocampal LTD in NMDA receptor epsilon 2 subunit mutant mice. *Neuron.* 1996;16:333-344.

23. Cai L, Liow J-S, Morse CL, et al. Evaluation of 11C-NR2B-SMe and its enantiomers as PET radioligands for imaging the NR2B subunit within the NMDA receptor complex in rats. *J Nucl Med.* January 10, 2020 [Epub ahead of print].

24. Shaw PJ, Eggett CJ. Molecular factors underlying selective vulnerability of motor neurons to neurodegeneration in amyotrophic lateral sclerosis. *J Neurol.* 2000;247 Suppl 1:I17-27.

25. Mallozzi C, Spalloni A, Longone P, Domenici MR. Activation of phosphotyrosine-mediated signaling pathways in the cortex and spinal cord of SOD1(G93A), a mouse model of familial amyotrophic lateral sclerosis. *Neural Plast.* 2018;2018:2430193.

26. Fuller PI, Reddrop C, Rodger J, Bellingham MC, Phillips JK. Differential expression of the NMDA NR2B receptor subunit in motoneuron populations susceptible and resistant to amyotrophic lateral sclerosis. *Neurosci Lett.* 2006;399:157-161.

FIGURE LEGENDS

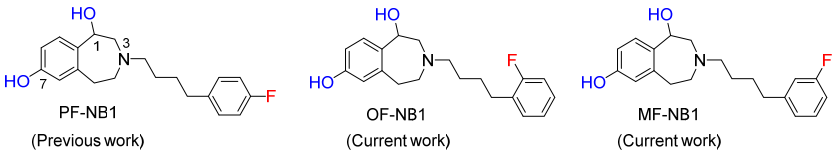

Figure 1. Structures of PF-NB1 and its regioisomers, OF-NB1 and MF-NB1 (*16*).

Table 1. Binding affinity (K_i) and selectivity profile of OF-NB1 and MF-NB1. The results are given as mean ± standard deviation for *n*=3

Compound	K_i (GluN2B) ± STD (nM)	K_i (σ1) ± STD (nM)	GluN2B/σ1 selectivity*
OF-NB1	10.4±4.7	410	39
MF-NB1	590±36	2700	4.6

*GluN2B selectivity was calculated as follows: K_i (σ1) / K_i (GluN2B)

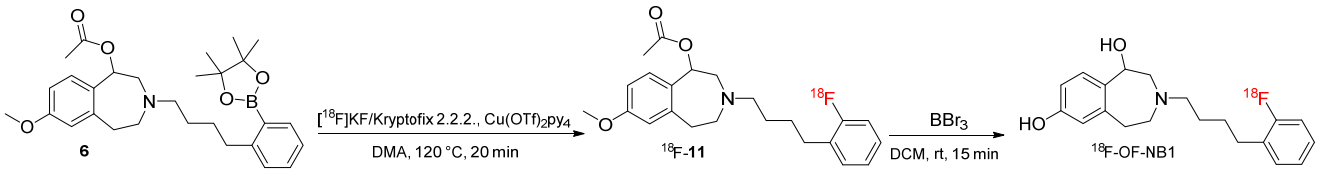

Figure 2. Representative radiosynthesis of ^{18}F-OF-NB1.

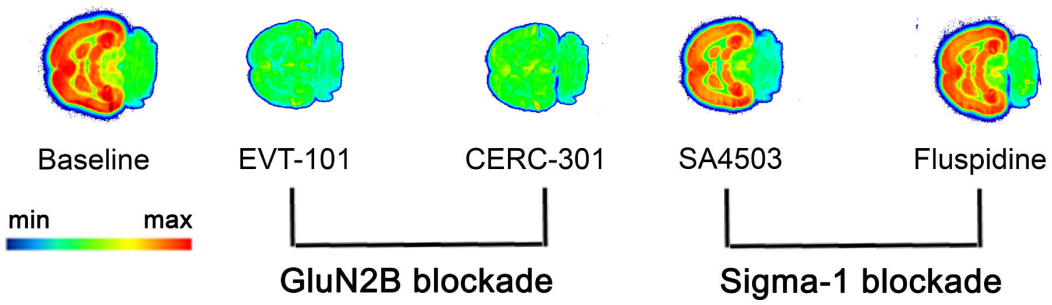

Figure 3. A typical *in vitro* autoradiogram of ^{18}F-OF-NB1 (3 nM) using rat coronal brain sections. GluN2B blockers and σ1R blockers were used to confirm specificity and selectivity, respectively. 1 μM solutions of GluN2B antagonists, EVT-101 and CERC-301 were used to determine specificity towards the GluN2B subunit, while 1 μM solutions of σ1R blockers, SA4503 and fluspidine, were used to confirm selectivity over σ1Rs.

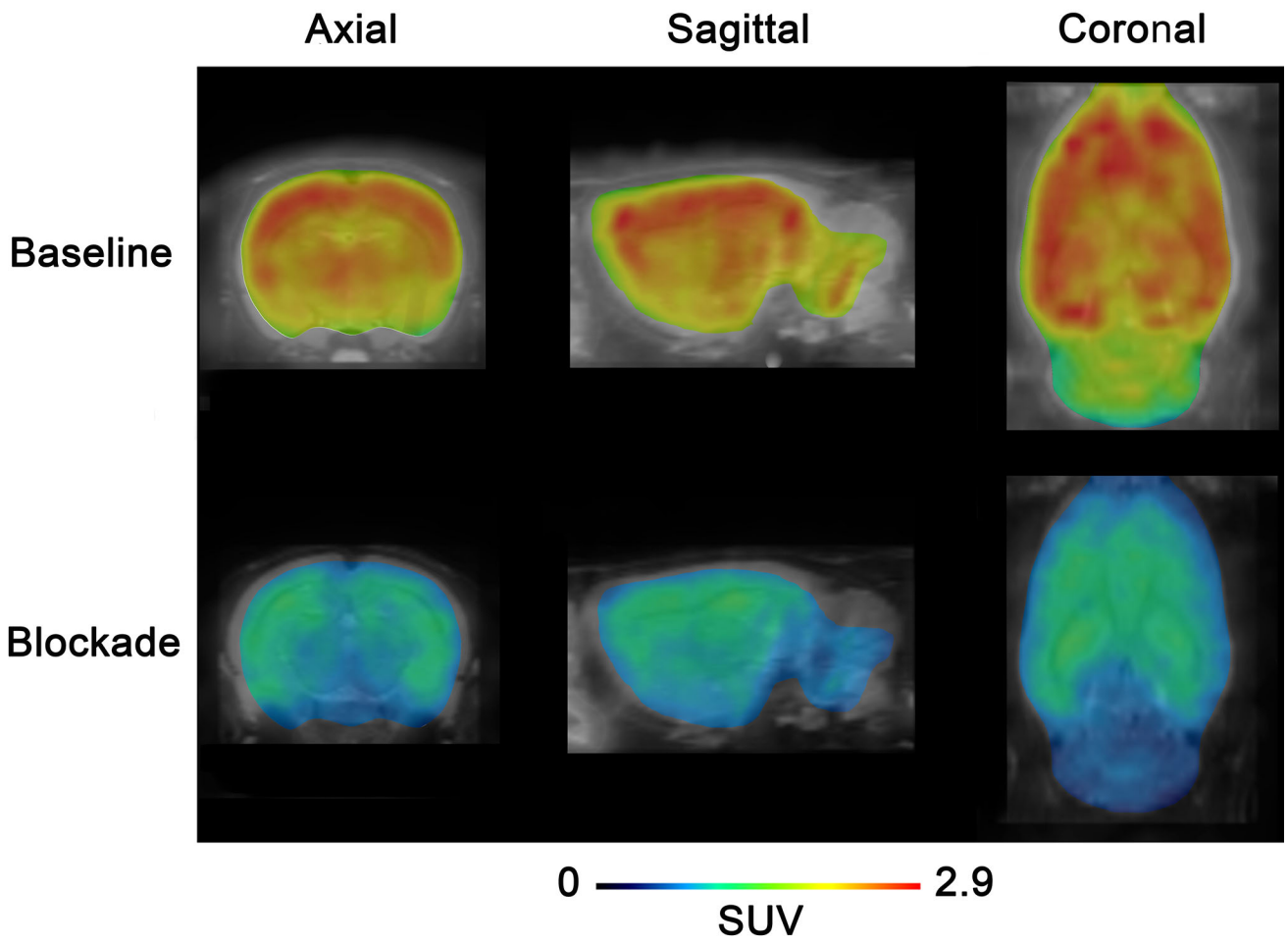

Figure 4. PET images of ^{18}F-OF-NB1 averaged over 30-90 min in rat brain under baseline and blockade (15 mg/kg CP-101,606) conditions superimposed on MRI T2 template (PMOD). The color bar points to min and max SUVs (calculated as accumulated radioactivity (Bq) per tissue (g) tissue and divided by injected dose per body weight).

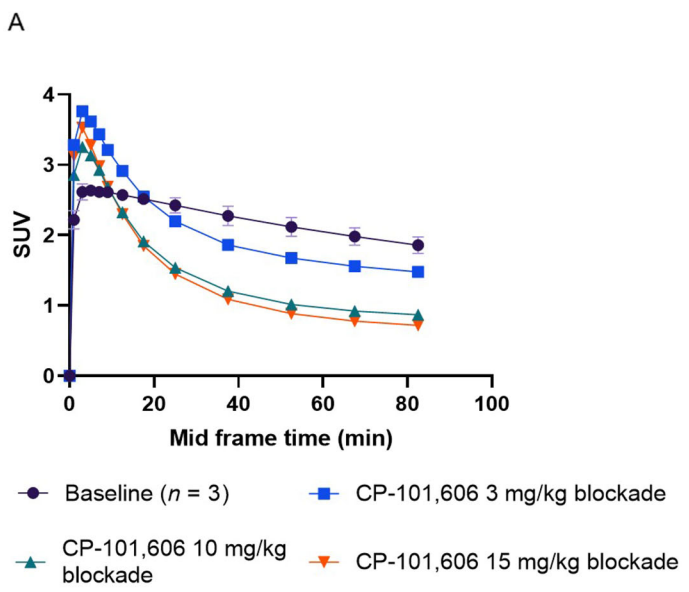

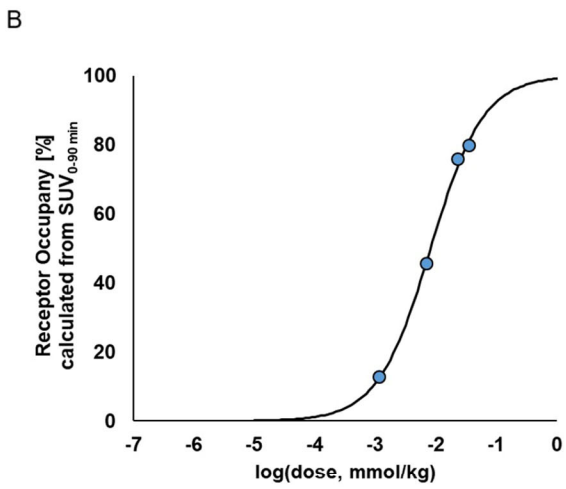

CP-101,606 mg/kg	%RO predicted	%RO calculated
0.5	13	13
3.0	46	46
10	74	76
15	81	80

Figure 5. A) TACs representing whole brain accumulation of ^{18}F-OF-NB1 presented as SUVs 0-90 min post-tracer injection under baseline conditions. TACs denoting blockade with GluN2B subunit antagonist, CP-101,606, with different doses (3, 10 and 15 mg/kg). B) RO of GluN2B subunit antagonist CP101,606 using ^{18}F-OF-NB1, in Wistar rats calculated from $SUV_{0\text{-}90\ min}$. D_{50} value of 8.1 µmol/kg was obtained using ^{18}F-OF-NB1. D_{50} is defined as the drug dose required to achieve 50% RO when administered and was calculated as previously outlined (*16*).

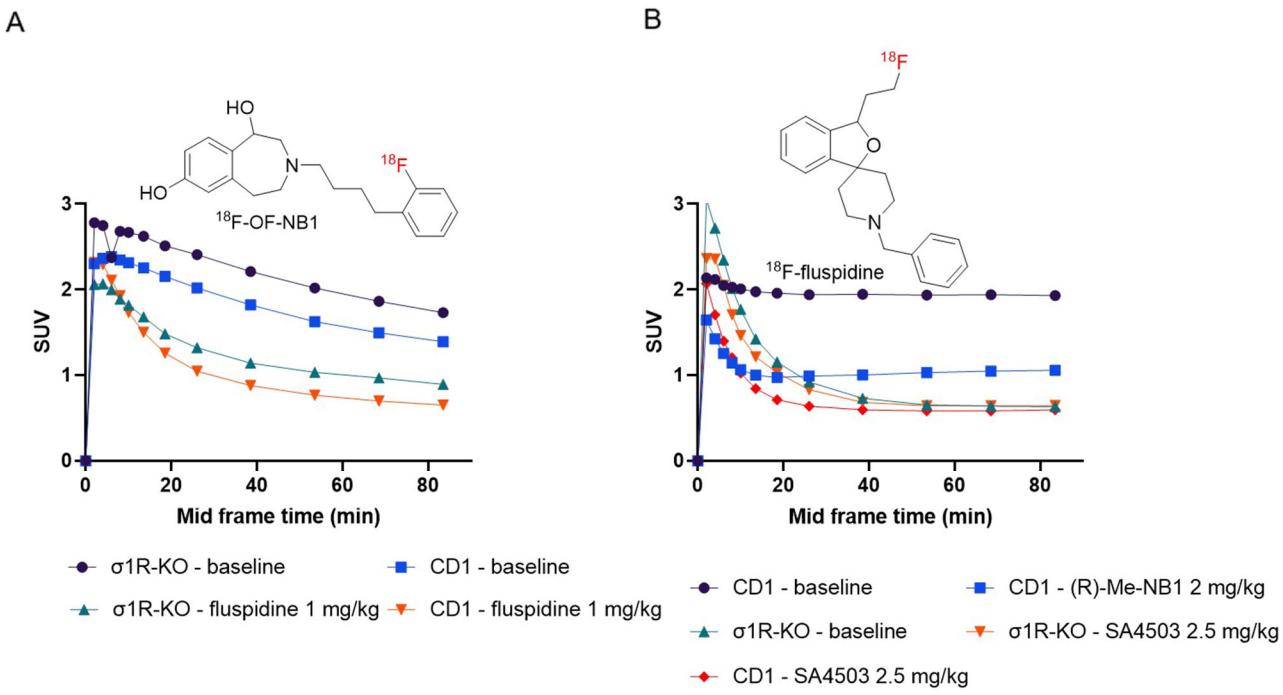

Figure 6. A) Whole brain TACs of ^{18}F-OF-NB1 (*n*=1 for each condition) in wild-type CD1 and σ1R-KO mice under baseline and blockade conditions with the σ1R agonist, fluspidine (1 mg/kg). B) Whole brain TACs of ^{18}F-fluspidine (*n*=1 for each condition) in CD1 and σ1R-KO mice under baseline and blockade conditions with the σ1R agonist, SA4503 (2.5 mg/kg) and GluN2B subunit ligand (*R*)-Me-NB1 in CD1 mice.

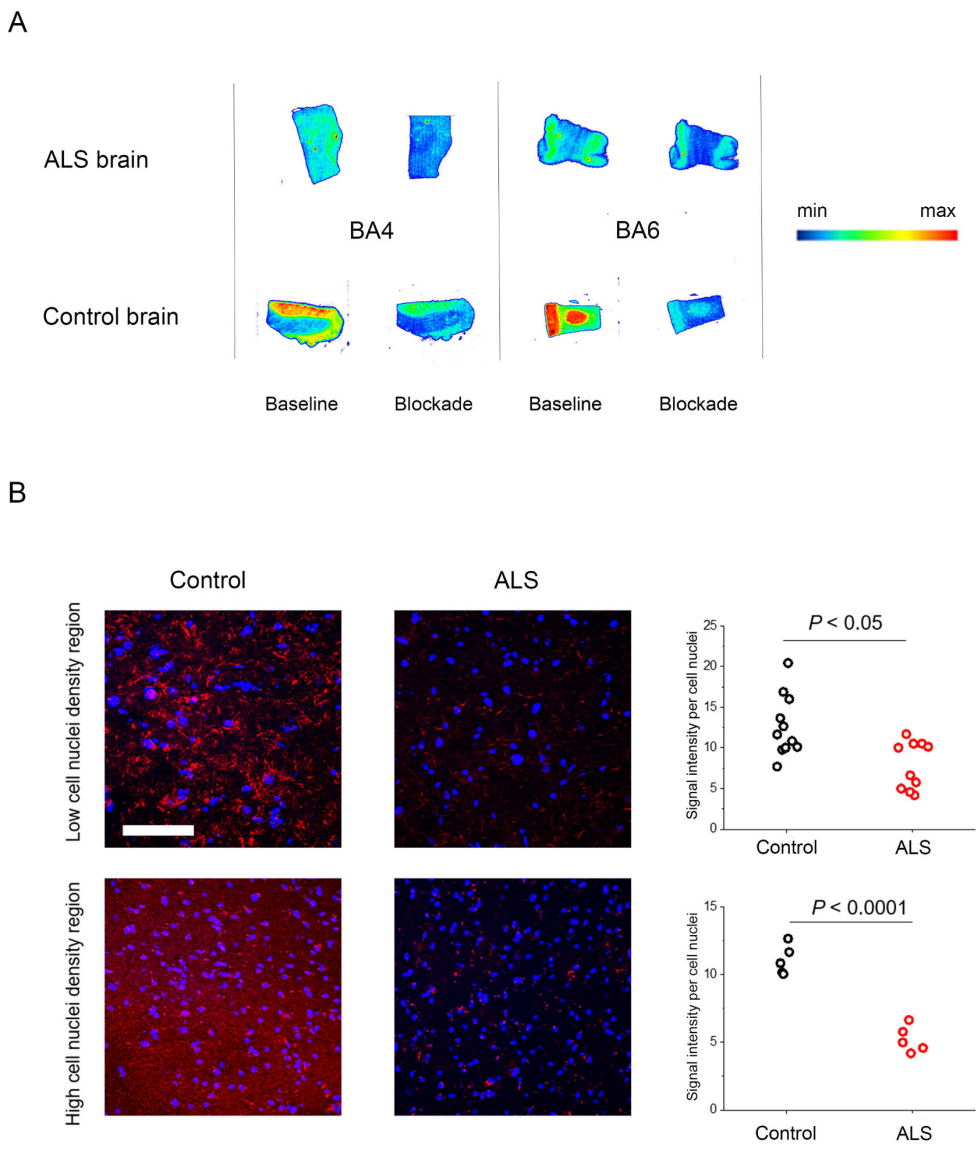

Figure 7. A) A typical *in vitro* autoradiogram of ^{18}F-OF-NB1 (3 nM) using human postmortem brain sections from ALS and non-ALS subjects. Blocking was achieved using 1 µM solution of GluN2B antagonist, CP-101,606. B) Comparative fluorescence immunostaining and confocal imaging of postmortem human brain cryosections shows relatively lower expression of GluN2B subunits (red) in an ALS patient compared to a non-ALS subject. Images were analyzed and graphically represented where each dot denotes one image. Nuclei are stained with DAPI (blue). Scale bar 100 µm.

Supplemental information for

Preclinical Development of ^{18}F-OF-NB1 for Imaging GluN2B-Containing N-Methyl-D-Aspartate Receptors and its Utility as a Biomarker for Amyotrophic Lateral Sclerosis

*Hazem Ahmed[1], Rahel Wallimann[1], Ahmed Haider[1], Vahid Hosseini[2], Stefan Gruber[1], Marvin Robledo[1], Thi A. N. Nguyen[1], Adrienne Müller Herde[1], Irina Iten[1], Claudia Keller[1], Viola Vogel[2], Roger Schibli[1,3], Bernhard Wünsch[4], Linjing Mu[1,3], Simon M. Ametamey[1]**

[1]Institute of Pharmaceutical Sciences, ETH Zurich, Vladimir-Prelog-Weg 4, CH-8093 Zurich, Switzerland

[2]Laboratory of Applied Mechanobiology, Institute of Translational Medicine, Department of Health Sciences and Technology, ETH Zürich, Vladimir-Prelog-Weg 4, CH-8093 Zurich, Switzerland

[3]Department of Nuclear Medicine, University Hospital Zurich, CH-8091 Zurich, Switzerland

[4]Institute of Pharmaceutical and Medicinal Chemistry, University of Münster, D-48149 Münster, Germany

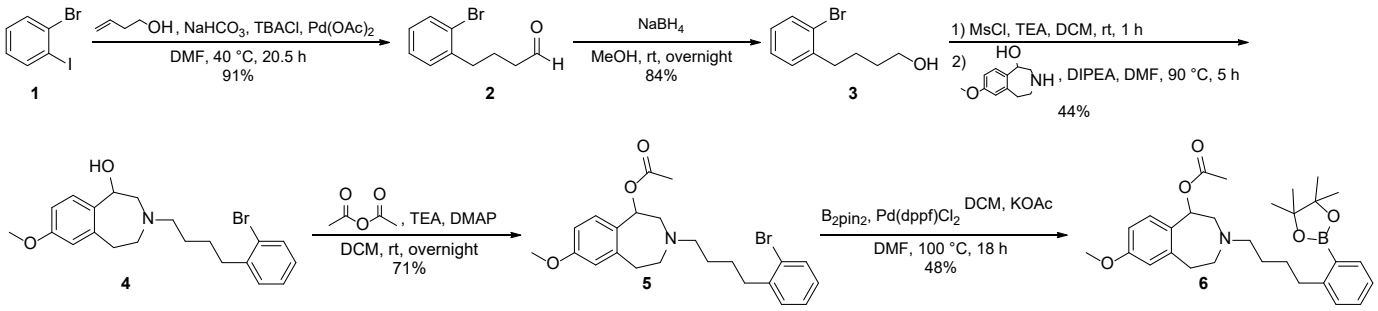

Supplemental Figure 1. Synthesis of boronic ester precursor **6** for synthesis of ^{18}F-OF-NB1.

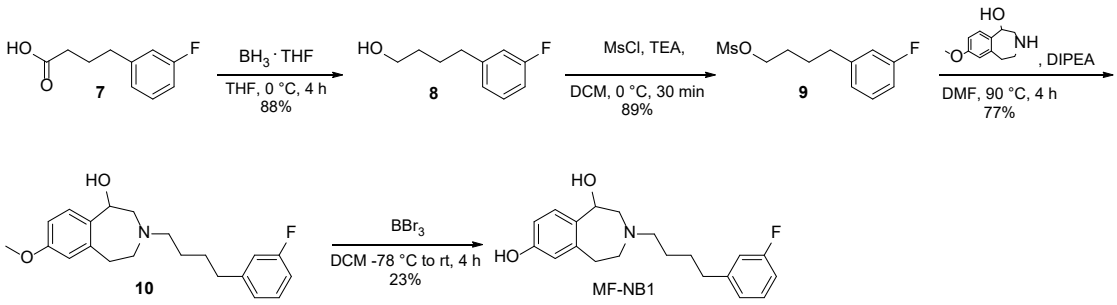

Supplemental Figure 2. Synthesis of MF-NB1.

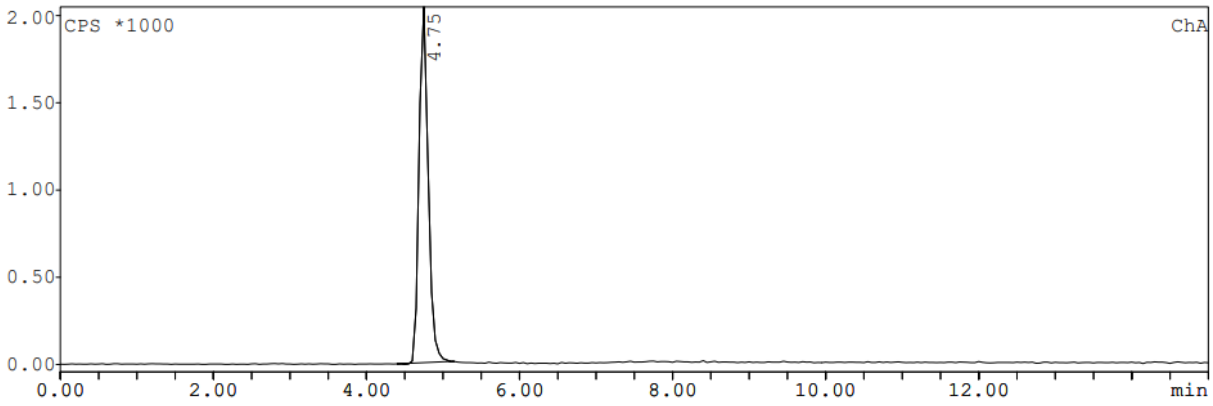

Supplemental Figure 3. Quality control of ^{18}F-OF-NB1 after formulation. In brief, ^{18}F-fluoride ions were produced by the bombardment of 98% enriched ^{18}O-water by means of the ^{18}O(p,n)^{18}F nuclear reaction in a Cyclone 18/9 cyclotron (18-MeV; IBA) resulting in a starting activity of nearly 60 GBq in 0.94 mL of ^{18}O-enriched H_2O. [^{18}F]fluoride ions were captured on an anion-exchange cartridge (Waters SepPak Accell QMA cartridge, light carbonate, preconditioned) and were then eluted with a mixture of Kryptofix 222 (6.3 mg/mL, 16.7 µmol/mL; Merck), $K_2C_2O_4$ (1.0 mg/mL, 5.4 µmol/mL), and K_2CO_3 (0.1 mg/mL, 0.7 µmol/mL) dissolved in a solution of MeCN/H_2O (4:1, 6 x 0.15 mL), followed by azeotropic drying with acetonitrile (3 x 0.8 mL) in a borosilicate glass Reacti-Vial (Wheaton Industries, 6 mL) sealed with a screw plastic cap in which a Teflon (DuPont)-faced rubber septum was fitted. The Reacti-Vial was subsequently left to cool down for 2 min and purged with air (20 mL), after which the residue was redissolved in a solution of 6–8 mg (18–24 µmol) of boronic ester **6** and 14 mg (21 µmol) of $Cu(OTf)_2(py)_4$ in 0.3 mL of dry dimethylacetamide. The mixture was stirred at 120 °C for 20 min before it was diluted with 35 mL of H_2O and the subsequent trapping of the intermediate on a C18 Plus cartridge (Waters, pre-conditioned with 5 mL MeCN and 5 mL H_2O). The cartridge was washed with water (5 mL) followed by the elution of radiolabeled protected intermediate **11** with 2 mL of EtOH which was evaporated at 95 °C for 6 min and subsequently azeotropically dried with MeCN (2 x 0.8 mL). The Reacti-Vial was cooled down in an ice bath before 0.5 mL of dichloromethane were added, followed by 1 mL of BBr_3 (1 M in DCM) and stirring at room temperature for 15 min. The dichloromethane was evaporated and the reaction was then quenched by the addition of aq. 0.1% H_3PO_4/MeCN (5:1, 3 mL). Afterwards, the products were purified by semi-preparative HPLC on a Merck-Hitachi L2130 HPLC system mounted with a radiation detector VRM 202 (Comecer, Netherlands). The purification was performed using an Agilent Eclipse XDB-C18 reversed phase

column (5 µm, 9.4 x 250 mm) and a gradient system comprising MeCN (solvent B) and aq. H_3PO_4 (0.1%, solvent C) with a flow rate of 4 mL/min and UV detection wavelength λ of 230 nm: 0.0-5.0 min, 20% B; 5.1-25.0 min, 20-40% B; 25.1-28.0 min, 40% B; 28.1-30.0 min, 40-60% B; 30.1-33.0 min, 60-90% B; 33.1-36.0 min, 90% B; 36.1-38.0 min, 90-20% B; 38.1-42.0 min, 20% B. The collected fraction was diluted with 35 mL of H_2O and the product was trapped on a C18 Light cartridge (Waters, pre-conditioned with 2 mL EtOH and 2 mL water). The cartridge was washed with 2 mL of water followed by elution of the radiotracer with 1 mL of EtOH. The product was formulated with 5% EtOH in water for injection to afford ^{18}F-OF-NB1. The identity of the radiotracer was confirmed by co-injection with its corresponding non-radioactive reference compound whereby an aliquot taken from the final formulation was injected into an Agilent 1100 HPLC system equipped with a Raytest Gabi Star radiodetector as well as an analytical Atlantis T3 C18 reversed-phase column (3 µm, 4.6 x 150 mm). A flow rate of 1 mL/min and detection wavelength λ of 230 were in use with a gradient system comprising 0.1% TFA in H_2O (solvent A), MeCN (solvent B); 0.0-10.0 min, 40-60% B; 10.01-11.00 min, 60-40% B; 11.01-15.0 min, 40% B.

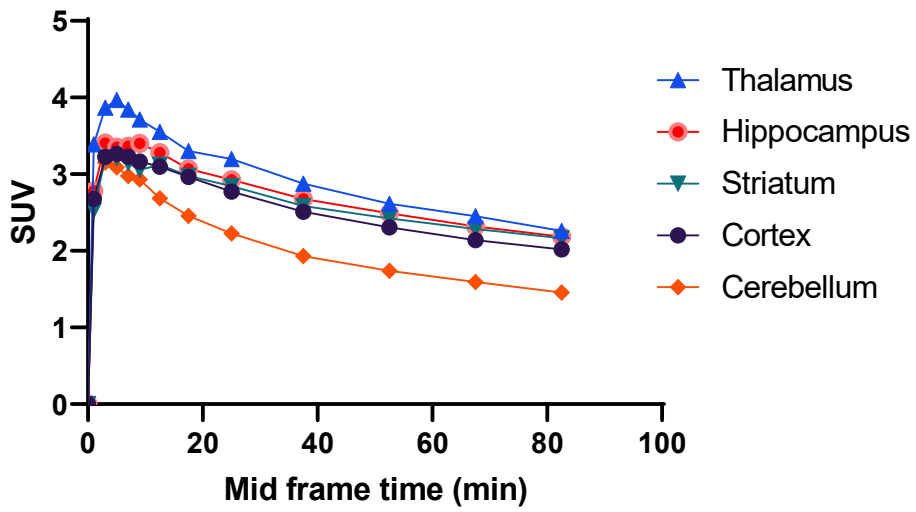

Supplemental Figure 4. Representative regional distribution of ^{18}F-OF-NB1 across the brain of a Wistar rat. The following equations were used simultaneously to determine the receptor occupancy from $SUV_{0\text{-}90\ min}$: - 1) $AUC = (b_{max} - b_{min}) * D_{50} / (D + D_{50}) + b_{min}$. 2) $RO = (b_{max} - AUC) / (b_{max} - b_{min}) * 100$, where AUC is defined as the area under the curve of the whole respective PET scan, D is the administered dose while RO is the receptor occupancy in %. B_{max} and b_{min} are the maximum and minimum binding values, respectively. For the autoradiography, adult rat brain tissues embedded in optimal cutting temperature medium were developed as 10 µm thick coronal sections on a cryostat (Cryo-Star HM 560 MV; Microm, Thermo Scientific, Wilmington, DE, USA). Slices were adsorbed on SuperFrost Plus glass slides (Menzel, Braunschweig, Germany) and subsequently preserved at -20 °C. The slices were thawed for 15 min on ice and subsequently preconditioned in an aqueous incubation buffer consisting of 30 mM HEPES, 0.56 mM $MgCl_2$, 110 mM NaCl, 5 mM KCl, 3.3 mM $CaCl_2$ and 0.1 % fatty acid free bovine serum albumin (pH 7.4, 0 °C) for 10 min. The slides were allowed to dry for 2-3 min at room temperature and then incubated with 3 nM of ^{18}F-OF-NB1, either alone or premixed with GluN2B subunit or σ1R blockers for 20 min at room temperature in a humidified chamber. The liquid was decanted and the slices were left for 5 min in the incubation buffer at 0 °C. The slices were washed (2 x 3 min) in a washing buffer (Same composition as the incubation buffer but without the fatty acid free bovine serum albumin) and (2 x 5 sec) in distilled water at 0 °C. The slices were subsequently dried for 5 min at room temperature and then exposed to a phosphor imager plate (Fuji, Dielsdorf, Switzerland) for 35-40 minutes. The films were scanned by a BAS5000 reader (Fuji) and the data was analyzed using AIDA 4.50.010 software (Raytest Isotopenmessgeräte GmbH, Straubenhardt, Germany).

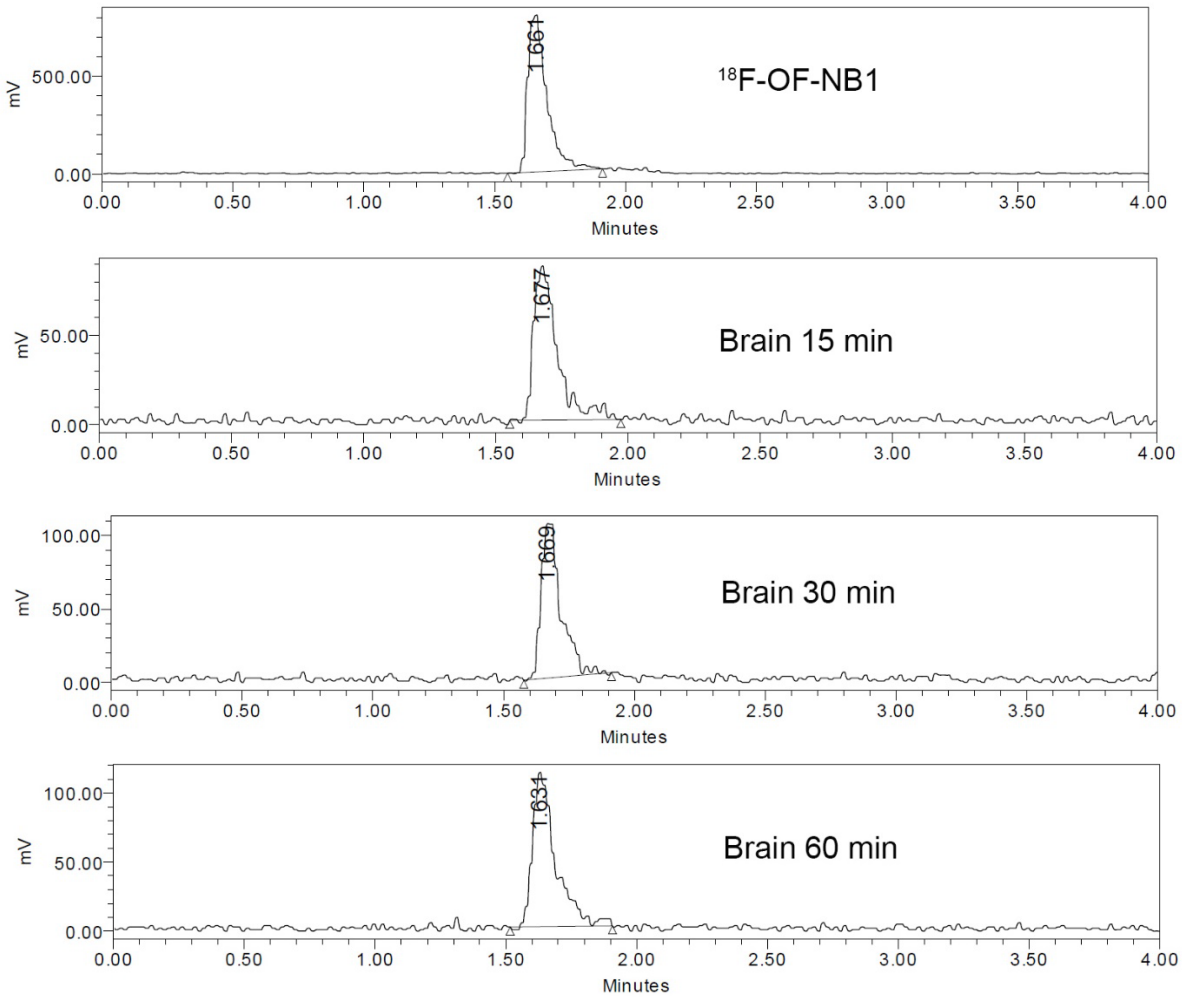

Supplemental Figure 5. *Ex vivo* metabolite study with ^{18}F-OF-NB1 in male Wistar rats. Radio-UPLC analysis of brain homogenate samples after 15, 30 and 60 min post-injection showed the exclusive presence of the parent intact tracer. In brief, the brain extracts were dissolved in 2 mL phosphate buffered saline (PBS) followed by homogenization and subsequent addition of 2 mL acetonitrile. Afterwards, the mixture was vortexed, centrifuged at 5000g for 5 min (4 °C) and the resultant supernatant was filtered. The blood samples were collected in heparin-coated tubes followed by transfer of 0.1 mL of the sample to Eppendorf tubes containing acetonitrile. The Eppendorf tubes were vortexed and centrifuged at 5000g for 5 min at 4 °C resulting in plasma supernatant. The supernatant was collected into new Eppendorf tubes containing acetonitrile and subsequently followed by a second centrifugation. The resultant supernatant was filtered. The processed brain and blood samples were analyzed by radio-ultra-performance liquid chromatography (UPLC).

Supplemental Table 1. Brain biodistribution of ^{18}F-OF-NB1 in Wistar rats (baseline injections n=4, eliprodil 2 mg/kg blockade n=4), reported as averaged % normalized injected dose per gram body weight ± SD. For blockade experiments, 2 mg/kg of eliprodil constituted in a solution of aqueous glucose (5%), NaCl (0.45%) and citric acid (1 mM) was administered prior to tracer injection. Organs were extracted, weighed and radioactivity was measured in a gamma-counter (Perkin Elmer, Schwerzenbach, Switzerland). For statistical analysis, an independent two-tailed paired Student's test assuming normal distribution of the dataset was employed to determine statistical probability values.

Organ	**45 min post-injection**	**45 min post-injection + 2 mg/kg eliprodil**	**Specificity %**
Bulbus olfactorius	0.24 ± 0.04	0.11 ± 0.007	53
Hippocampus	0.24 ± 0.02	0.17 ± 0.012	31
Thalamus	0.29 ± 0.04	0.17 ± 0.011	42
Cerebellum	0.23 ± 0.02	0.11 ± 0.007	52
Brain stem	0.28 ± 0.04	0.12 ± 0.009	55
Colliculus superior/inferior	0.29 ± 0.03	0.12 ± 0.009	57
Cortex	0.32 ± 0.04	0.16 ± 0.010	52
Striatum	0.29 ± 0.03	0.15 ± 0.008	48

Supplemental Table 2. *Ex vivo* whole body biodistribution of ^{18}F-OF-NB1 in Wistar rats (baseline injections n=4, eliprodil 2 mg/kg blockade n=4), reported as averaged % normalized injected dose per gram body weight ± SD.

Organ	**45 min post-injection**	**45 min post-injection + 2 mg/kg eliprodil**	**Specificity %**
Spleen	0.27 ± 0.02	0.22 ± 0.017	19
Liver	0.10 ± 0.02	0.13 ± 0.017	No specificity
Kidney	0.62 ± 0.05	0.25 ± 0.018	59
Adrenal gland	1.4 ± 0.21	0.42 ± 0.054	69
Lungs	0.30 ± 0.04	0.22 ± 0.041	28
Bone	0.08 ± 0.01	0.07 ± 0.007	13
Heart	0.08 ± 0.01	0.06 ± 0.003	27
Fat	0.03 ± 0.005	0.04 ± 0.008	No specificity
Intestine	0.64 ± 0.08	0.77 ± 0.270	No specificity
Testicles	0.07 ± 0.01	0.07 ± 0.004	0.05
Blood	0.01 ± 0.001	0.01 ± 0.001	No specificity
Urine	0.55 ± 0.18	0.70 ± 0.082	No specificity
Muscle	0.08 ± 0.01	0.07 ± 0.006	16
Pancreas	0.72 ± 0.03	0.61 ± 0.035	16
Skin	0.04 ± 0.005	0.04 ± 0.003	3